Journal of Cleaner Production 248 (2020) 119274

Contents lists available at ScienceDirect

Journal of Cleaner Production

journal homepage: www.elsevier.com/locate/jclepro

A novel composite silver nanoparticles loaded calcium oxide stemming from egg shell recycling: A potent photocatalytic and antibacterial activities

Ibrahim Hotan Alsohaimi [a, *], Amr Mohamed Nassar [a, b, **], Tarek Ahmed Seaf Elnasr [a, c], Ben amar Cheba [d, e]

[a] Chemistry Department, College of Science, Jouf University, Sakaka, Saudi Arabia
[b] Chemistry Department, Faculty of Science, Al-Azhar University, Nasr City, 11884, Cairo, Egypt
[c] Department of Chemistry, Faculty of Science Al-Azhar University, Assiut, 71524, Egypt
[d] Biology department, College of Science, Jouf University, Sakaka, Saudi Arabia
[e] Department of Biotechnology, Faculty of Nature and Life Sciences, University of Sciences and Technology of Oran -Mohamed Boudiaf (USTOMB), BP 1505 Al Mnaouar, Oran, 31000, Algeria

ARTICLE INFO

Article history:
Received 23 August 2019
Received in revised form
5 October 2019
Accepted 11 November 2019
Available online 12 November 2019

Handling editor: Baoshan Huang

Keywords:
Egg shell
Recycling
Sustainable
Silver nanoparticles
Photocatalyst
Antibacterial

ABSTRACT

Industrial wastewater resulted from textile dyeing process is considered as a big environmental problem. Therefore, recycling of wastewater offers environmental and economic values specially if the materials used are resulted from recycling of other kinds of waste. From this point of view and for the first time this work deals with the study the wastewater recycling by calcium oxide resulted from eggshell recycling. Calcium oxide (CaO) nanocrystals were created by the thermal annealing of chicken egg shell at 1100 °C for 2 h s. Heat treatment at 200 °C in air for 2 h s of the resulted CaO with silver oxalate gave the novel composite, silver nanoparticles loaded calcium oxide (Ag-NPs @ CaO). By applying electronic spectra (UV−Vis), Fourier transform infrared spectroscopy (FT-IR), X-ray diffraction (XRD), scanning electron microscopy with the energy dispersion spectrum analysis (SEM-EDX) and transmittance electronic microscope (TEM), the materials were characterized. The energy band gap was calculated from the equation of Tauc for CaO and Ag-NPs@CaO and measured to be 2.1 and 2 eV, respectively. Indigo carmine (IC) as a model of photocatalytic decolorization was performed using both CaO and Ag@CaO nanoparticles under sunlight exposure. The impacts of various variables such as solution pH, dose quantity, temperature and irradiation time were studied. Both catalysts displayed an effective photocatalytic activity in IC decolorization but Ag@CaO composite displayed a stronger activity than CaO. The percentages of dye degradation were ≈99.21% and 99.45% in case of CaO and Ag@CaO, respectively. The antibacterial efficiency was measured against some Gram-negative and Gram-positive bacteria. Ag@CaO provided powerful weapons against the drug-resistant bacteria. These findings give a promising and economic strategy for all those who are interested in industries which involve dyeing process.

1. Introduction

Circular economy nowadays is the goal for research that seeks improvement in sustainable development. It aims at minimizing human and industrial pollution by turning waste and by-products into eco-friendly products. Egg shell is one of the global solid waste materials. There is a huge amount of eggshell waste worldwide (≈8 million ton/year) (Gabriele et al., 2017). Although egg shell is low-risk waste (category 3) (Evangelia et al., 2018), it is considered as a pollution source, because it is disposed directly in environment. Egg shell is considered to be a biomineralized material of calcium carbonate crystals embedded in fibres of protein matrix, which occupies about 11% of the whole egg weight (Oliveira et al., 2013). The presence of organic protein framework in egg shell makes it a valuable goal for rats and worms which results in a

* Corresponding author. Chemistry Department, College of Science, Jouf University, Sakaka, Saudi Arabia.
** Corresponding author. Chemistry Department, College of Science, Jouf University, Sakaka, Saudi Arabia.
E-mail addresses: ehalshaimi@ju.edu.sa (I.H. Alsohaimi), amnassar@ju.edu.sa (A.M. Nassar).

https://doi.org/10.1016/j.jclepro.2019.119274
0959-6526/

problem for human health (Khemthong et al., 2012). $CaCO_3$ is the basic content of egg shell (Elaheh, 2013). It can be converted to calcium oxide (CaO) by thermal treatment at 900 °C (Witoon, 2011). The physical properties of CaO such as crystal size and specific surface area, which are substantial factors in photocatalytic process, can be modified upon annealing (Song and Zhang, 2010). It has been reported that, when annealing temperature increased, the surface area deceased due to the particle size decreased (Kim and Park, 2001). Therefore, to attain the largest photodegradation activity, it is essential to find the optimum temperature. At 800 °C and 1000 °C, CaO possessed a lower surface area (Peralta et al., 2018). CaO shows potential heterogeneous catalytic activity, it has tolerance of moisture, inexpensive, non-corrosive, able to be reused and is environmental friendly (Boey et al., 2011). CaO is a photoactive compound (Song et al., 2009) used to degrade many organic contaminants (Devarahosahalli Veeranna et al., 2014; Shaveisi and Sharifnia, 2018). Calcium oxide resulted from calcination of egg shell was used in different sectors such as biocatalyst, adsorbent for capturing of heavy metals, fertilizer and precursor for synthesis of composite dielectric materials (Colombo et al., 2017).

Although Indigo carmine dye (IC) is used in many application fields, such as textile industry as a dying agent; in analytical chemistry as a redox indicator; in medicine as pharmaceutical ingredients and in biology as microscopic stain (Oppong et al., 2019), it is categorized as environmentally hazard material because the discharge of its wastewater causes high toxicity for the organisms in addition to its highly blue color which causes esthetic pollution (Szoke et al., 2019).

Visible-light photocatalysis, using sunlight irradiation as a light source in wastewater remediation and environmental protection, has been regarded as a green and an effective technology. Thus, the manufacturing of visible light semiconductors through an easy, green and economic strategy seems to be very important and essential.

Recently, many scientists have concentrated on manufacturing of economic materials through the process of waste recycling that is applicable for wastewater treatment (Maroušek et al., 2019a). Lorena et al. studied the photocatalytic degradation of methylene blue and rhodamine, B using zinc/manganese blended oxide catalysts generated from black mass spent alkaline batteries (Lorena et al., 2019). The band gap magnitude for the metal oxides were in the range of 1.32–1.38 eV, while in the range 3.10 and 3.20 eV for zinc oxide samples. The percentages of photocatalytic degradation were more than 70% and 50% for methylene blue and rhodamine B, respectively. Polystyrene obtained from waste plastic was used to manufacture SnO_2 impregnated polystyrene foams that were used to remediate waste water and showed very excellent effectiveness. The proportion of removal of dye reaching up to 98.2 percent under UV light (Geovania et al., 2018). A low-cost TiO_2–NPs@egg shell membrane composite was manufactured by an easy self-assembly technique as a reusable photocatalyst for organic color decomposition. The composite demonstrated notable photocatalytic activity against dye solution degradation under light xenon lamp irradiation (Yaling et al., 2017). Waste polystyrene particles were used as an efficient photocatalytic material to fabricate TiO_2-NPs@polystyrene composite. The photocatalyst showed highly promising reduction of Cr(VI) and methylene blue organic dye removal as pollutant models. An antimicrobial action against E. Coli and A. Niger as microorganisms models was also demonstrated as the biological activity of the composite (İlknur, A. Münevver, S. 2014).

Our goal in this research is to accomplish two objectives by converting chicken egg shell waste collected at no cost into cheap precious wastewater treatment material. First of all, the calcination of egg shells is used to create CaO nanocrystals followed by the synthesis of their modified novel composite Ag-NPs@CaO. Secondly, the composite was examined for environmental purpose by evaluating its semi-conductive features as photocatalysts in indigo carmine decoloration in aqueous solution under sunlight irradiation and by evaluating its antimicrobial efficacy. Finally, this work was the first research dealing with the egg shell calcination product as a photocatalyst under solar irradiation.

2. Experimental

2.1. Materials

The used materials are chicken eggshells which were collected at no cost from local restaurant in Sakaka Aljouf. Silver nitrate, oxalic acid and indigo carmine dye purchased from Sigma-Aldrich (Spruce Street, St. Luis, USA) and used as mentioned earlier. All aqueous solutions were prepared from Milli Q water.

2.2. Instruments

The used instrument for performing the infrared spectra (IR) was IR Tracer-100 Fourier Transform Infrared (FTIR) spectrometer, Shimadzu, Japan. Electronic spectra were recorded using electronic spectra were obtained using a LABOMED – spectro UV–Vis double beam-3200 in the range (195–1100 nm). XRD measurements were carried out using an X-ray Diffractometer, XRD-7000, Shimadzu, Japan with a Cu detector using 1.54 Å wavelength. XRF measurements were processed using an X-Ray Fluorescence Spectrometer (XRF-1800), Shimadzu, Japan. TEM images of samples were performed using scanning electron microscopy (JEOL, JEM-2100, Japan). The morphological and the elemental analysis of the samples were explored and investigated with an ultra-high resolution FE-SEM microscope (JSM5410JEOL) coupled with energy dispersive X-ray spectrometer (EDX). TEM images were recorded by scanning electron microscopy (JEOL, JEM-2100, Japan).

2.3. Preparation of calcium oxide nanoparticles, CaO from chicken egg shell

CaO was prepared from eggshell as described before (Ferraz et al., 2018) with some modifications. Firstly, 50 g from the collected egg shells were rinsed by deionized water to get rid of the contaminants and kept in dry oven at 110 °C for 2 h s. Then, for 2 h s in a muffle furnace, the egg shells were calcined at 1100 °C. After calcination process the solid formed from CaO was cooled inside the furnace for 10 h, then stored in desiccator.

2.4. Fabrication of $Ag_2C_2O_4$

Silver oxalate was synthesized adopting the previous method (Navaladian et al., 2007). 50 mL from oxalic acid solution, 0.25M was added drop by drop to a 50 mL from silver nitrate solution, 0.50 M with continues stirring. The white solid formed from silver oxalate was separated, rinsed with warm water (3 × 10mL) and dried at room temperature.

2.5. Synthesis of Ag nanoparticles loaded calcium oxide, Ag-NPs@CaO

Silver oxalate, 1 g well mixed with calcium oxide, 3 g. The mixture was crushed in porcelain mortar until forming a fine powder. Then, the mixture was kept at furnace at 200 °C for 2 h s. The light brown solid obtained from Ag-NPs @ CaO was collected and stored in desiccator.

2.6. Photocatalytic activity estimation

Indigo carmine dye was used as a template to monitor the semiconductor CaO and Ag-NPs@CaO photocatalytic activity. In a quartz beaker (150 mL), 80 mg of the photocatalyst was added to 25 mg/L of IC solution (100 mL) and mixed at ambient temperature with a magnetic stirrer in the dark for 5 min to establish the equilibrium between the IC and the surface of catalyst. Then, the mixture was subjected to sun light irradiation 40×10^3 Lux (measured by PeakTech digital multi tester). Nearly 3 mL of the treated IC solution was taken and centrifuged for 5 min to separate the photocatalyst at a fixed interval of time. The percentage (%) of the purified IC solution was checked by calculating the absorbance (A) of the treated filtrate solution at 612 nm (λ_{max}) using UV–Vis spectrophotometer and calculated following Eq. (1):

$$\text{Decolorization efficiency } (\%) = \frac{\boldsymbol{A_0} - \boldsymbol{A_t}}{\boldsymbol{A_0}} \times 100 \quad (1)$$

A_0 is the initial of absorbance of the dye and A_t related to the absorbance of the treated IC after a given time. Control experiments without catalyst and in dark were also carried out. The photocatalytic reaction conditions such as catalyst quantity (dose), pH of solution and temperature were performed to optimize the photo decolorization process.

2.7. Antibacterial activity assay

The antibacterial activity of nanoparticles substances of CaO and Ag@ CaO was tested by agar-well diffusion method. Briefly, the bacterial isolations were cultivated in a nutrient broth medium containing 5 g/L of yeast extract, 10 g/L bactotryptone, and 10 g/L NaCl for 18 h at 37 °C. One hundred microliter of the cell suspensions were spread on a nutrient agar surface using sterilized cotton swabs and the agar medium was punched with 8 mm diameter wells and filled with 500ul of nanoparticles aqueous solutions (3 mg/ml). Subsequently the plates refrigerated for 2 h, and incubated at 37 °C for 18–24 h, the antibacterial activity of the samples, can be accessed via measuring the diameter of growth prevention halo (inhibition zone). The tested Bacteria were *Bacillus cereus, Bacillus subtilis, Enterococcus feacalis, E. coli, Klebsiella* sp., *Pseudomonas fluorescence, Enterobacter* sp., *and Micrococcus leteus* .

3. Results and discussion

3.1. Materials characterization

3.1.1. IR spectroscopy

The infrared spectra of egg shell calcination product and its silver loaded sample has presented a distinct band at 865 cm^{-1} which is due to Ca–O–Ca bonding identifies the presence of calcium oxide (Nassar et al., 2015). The sharp band observed at 3620 cm^{-1} is due to the ν (OH) of physisorbed water linked to nanoparticles (Hassan et al., 2013). The spectrum of the silver loaded CaO shows a weak peak at 780 cm^{-1} which may be due to interatomic vibration of Ag atom (Nassar et al., 2018).

3.1.2. XRD analysis

XRD assessment was used to examine the phase structures of the egg shell calcination product and its silver loaded sample. The data are presented in Fig. 1a and b, for CaO and Ag-NPs@CaO respectively. Obviously, the obtained diffraction pattern corresponding to the calcium oxide (CaO) pattern (JCPDS-82-1691) (Balázsi et al., 2007) (Fig. 1a). Furthermore, the peaks appear at $2\theta = 34.08$, 54.40, 62.44, 62.68 corresponding to (111), (220), (311) and (222) crystallographic planes of CaO, respectively. While, the diffraction peaks observed in Fig. 1b at 38.09, 44.28, 64.40, and 77.36 corresponding to (111), (200), (220), and (311) planes, respectively due to the formation of face-centered cubic silver nanoparticles (Nassar et al., 2019). The XRD patterns emphasized the crystalline structure of CaO and Ag@CaO. The average of crystalline size of the composite was calculated using Scherrer's formula (Nassar et al., 2019), Eq. (2):

$$D = k\lambda \,/\, \beta \mathrm{Cos}\theta \quad (2)$$

where, D is the average particle size, λ is the wavelength of Copper K-alpha radiation, β is the whole width of the diffraction peak, k is shape sensitive coefficient (0.9) and θ refers to the diffraction angle. The calculated average crystalline size found to be 24.27 nm and 57.38 nm for CaO and Ag@CaO, respectively.

3.1.3. XRF analysis

XRF findings indicate the purity of the products being synthesized. CaO sample findings show that it contains three components, calcium (Ca), oxygen (O), strontium (Sr) with 96.6938% CaO and 3.3062% SrO. The silver-loaded composite of calcium oxide indicates 68.7799% for CaO, 30.7036% for Ag and 0.2778% for SrO.

3.1.4. Morphological studies

Figs. 2 and 3 respectively show the SEM and TEM pictures of the synthesized compounds. The micrographs showed the materials ' semisphere structure. The influence of Ag nanoparticles on the surface of calcium oxide is illustrated as a decorated layer and due to more crystal growth, the composite has given more size. The TEM pictures indicate the 30–35 nm particle size for CaO and 60–70 nm particles size for Ag@CaO that matches XRD analysis well. EDX assessment, Fig. 4, verified the compounds. The calcination product of the egg shell has separate proportions of Ca, O, and C while the Ag-NPs@CaO has Ag as well as Ca, O, and C. The appearance of carbon may be due to some CO_2 air adsorption.

3.1.5. Band gap evaluation

Band gap energy of the photocatalysts was calculated from Tuac's equation (Rashad et al., 2014) (Eq. (3)):

$$\alpha h\nu = A(h\nu - Eg)^n \quad (3)$$

where Eg is the allowed energy band gap, α is the absorption coefficient, $h\nu$ is photon energy, A is a constant, $n = ½$ for allowed direct transition and $n = 2$ for allowed indirect transition. From the plot of $(\alpha h\nu)^2$ versus $h\nu$, the direct band gap can be calculated. The calculated values of energy band gap for Ag@CaO recorded 2 eV which is slight narrowing compared to CaO and (2.1 eV).

3.2. Photocatalytic performance

The photocatalytic activity of CaO and Ag@CaO was calculated by degrading IC dye using sun light irradiation with intensity 40×10^3 Lux. The chromophore absorption maxima in the absorption spectrum of IC is observed at λ_{max} 615 nm (Barka et al., 2008) and it was reduced in Fig. 5a and b for CaO and Ag@CaO catalysts, respectively. As shown, it takes 25 min for 25 ppm IC solution photocatalytic degradation with catalyst dose 0.80 g/L. The percentages of dye decolorization were ≈99.21% and 99.45% in case of CaO and Ag@CaO photocatalysts. respectively.

The reaction kinetics of sun irradiation as light source for IC photodegrdation was studied using Langmuir Hinshelwood model for first order kinetic (Essawy et al., 2018):

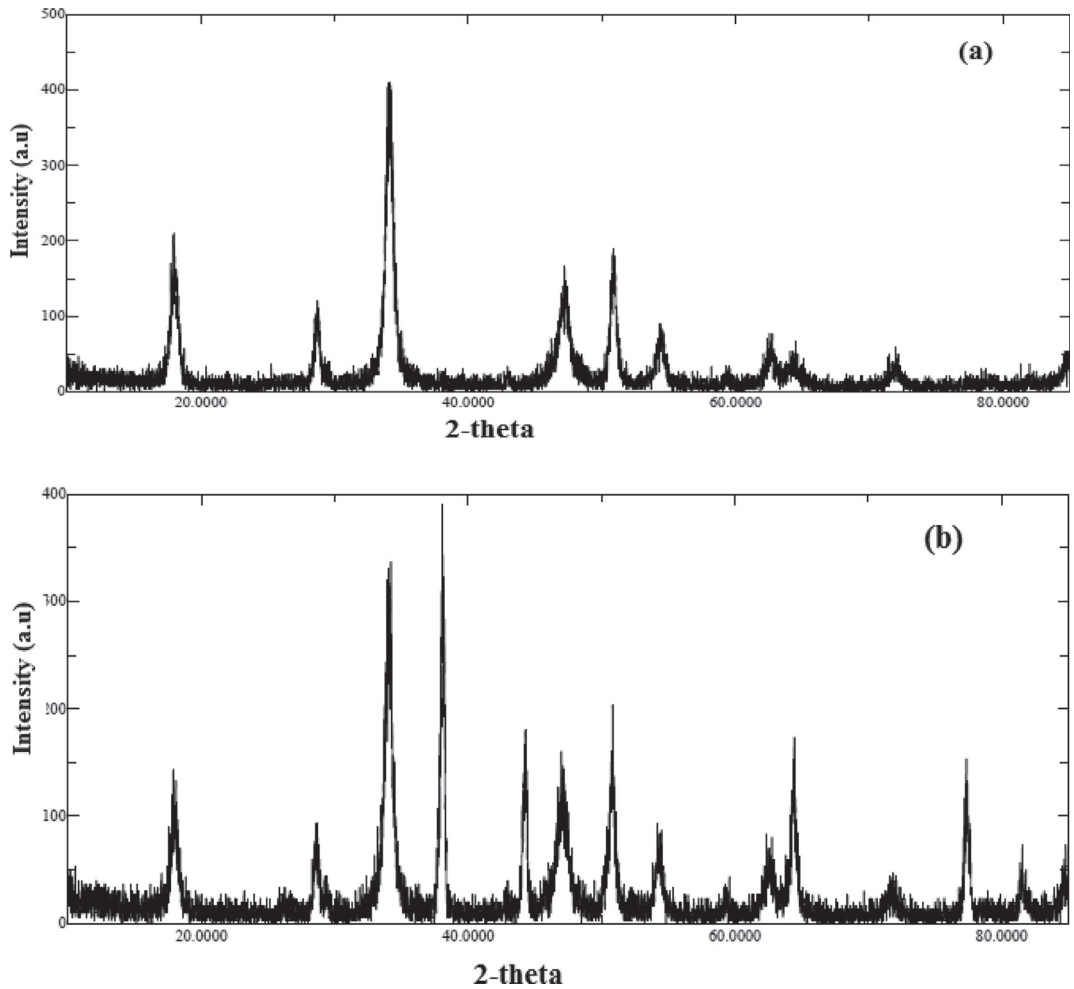

Fig. 1. XRD patterns of pure CaO (a) and Ag@CaO composite (b).

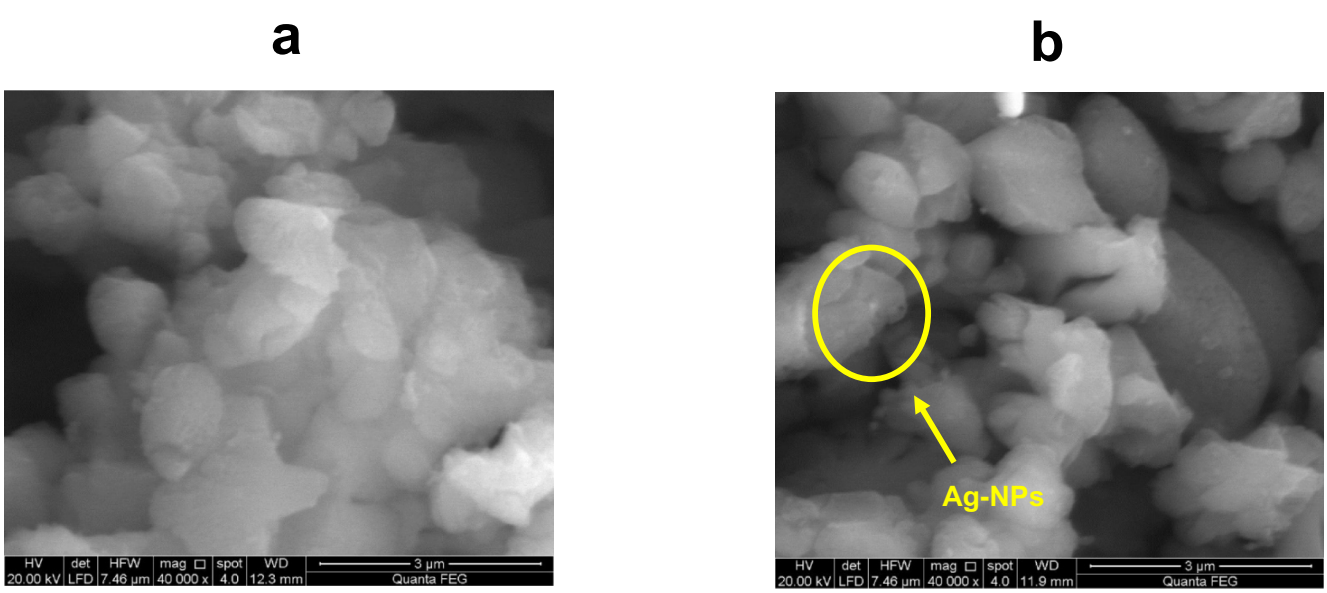

Fig. 2. SEM images of pure CaO (a) and Ag@CaO composite (b).

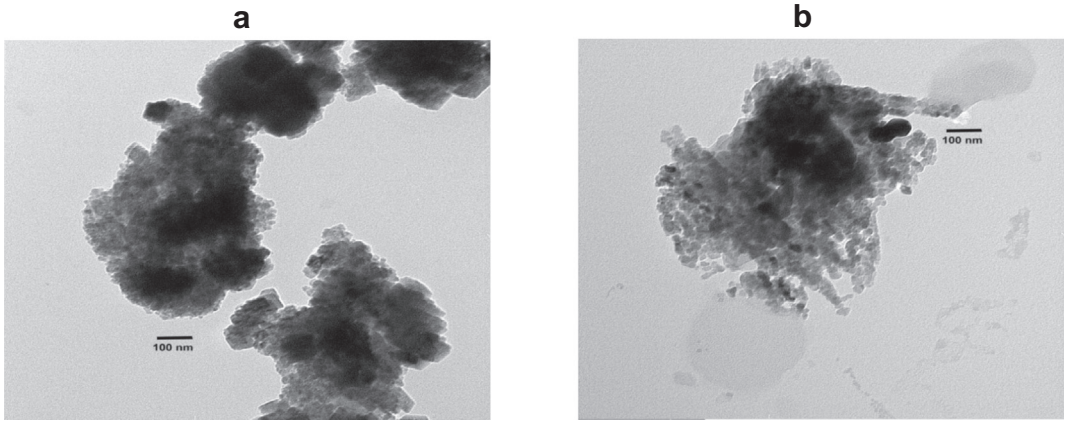

Fig. 3. TEM images of pure CaO (a) and Ag@CaO composite (b).

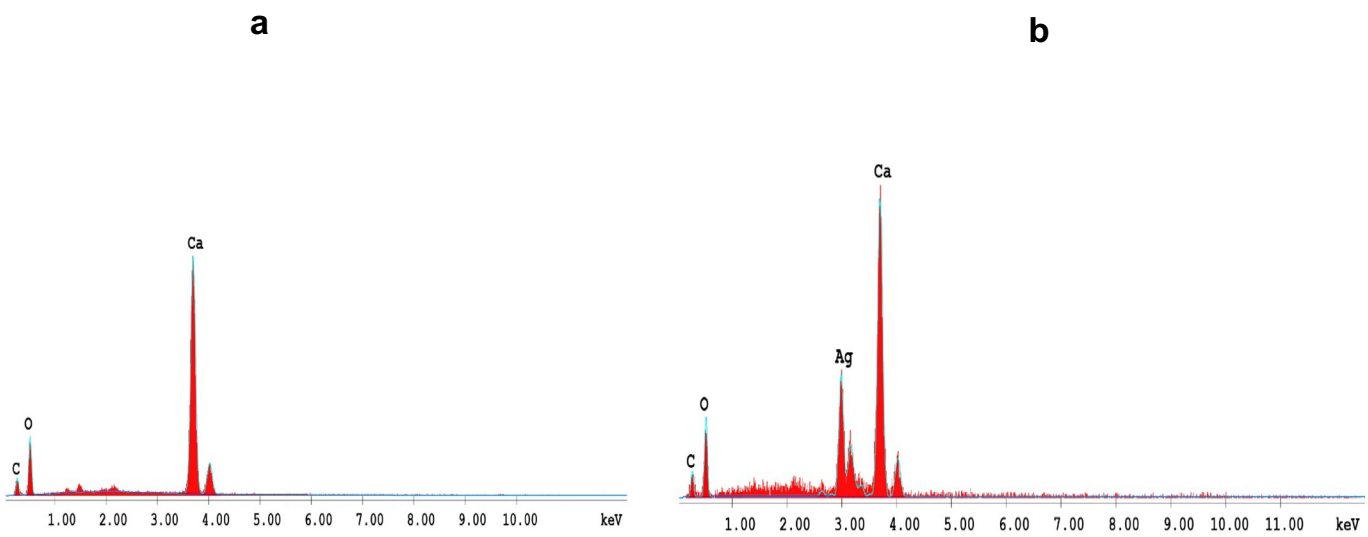

Fig. 4. EDX of pure CaO (a) and Ag@CaO composite (b).

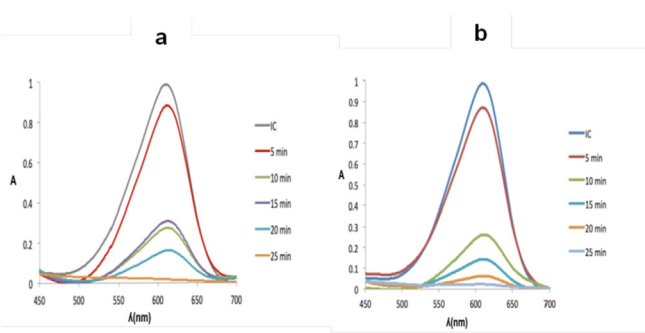

Fig. 5. Variation in absorption spectrum of solution of IC dye under different irradiation time Effect in the presence of pure CaO (a) and Ag@CaO composite (b).

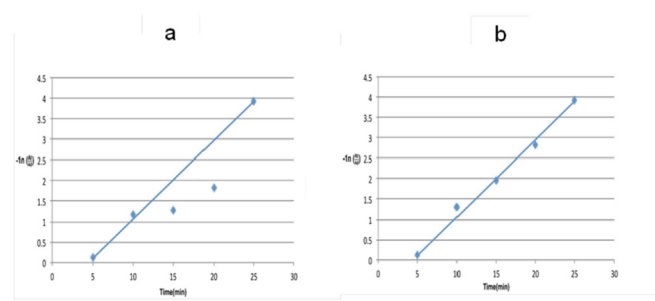

Fig. 6. Kinetic studies of the photocatalytic degradation of IC dye in the presence of pure CaO(a) and Ag@CaO composite (b).

$$-\ln\left(\frac{At}{Ao}\right) = kt$$

where, A_o is IC initial absorption, A_t is the IC absorption at t (time) and k is the rate constant. Fig. 6a and b shows the plot for -ln ($\frac{At}{A_0}$) versus time for both two catalysts. From the obtained results, it is well accepted that the decolorization of IC obeyed a pseudo first-order kinetic (Nassar, 2018). The rate constant k was obtained to be 0.16 min^{-1} and 0.18 min^{-1} for CaO and Ag@CaO, respectively. Silver nanoparticles enhanced light utilization, so the degradation rate in case of Ag@CaO is better than CaO.

Fig. 7 illustrates the absorption spectra of the dye after photolysis experiment in the absence of catalyst, the effect of catalyst only without light and the effect of the catalyst in the presence of sun light. It can be observed that in the absence of Ag@CaO, no decolorization occurred. Adsorption experiment was also conducted in

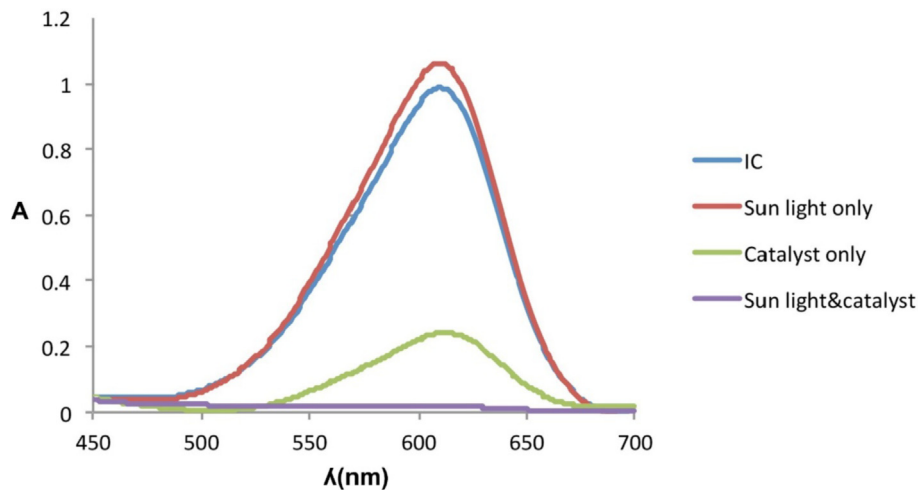

Fig. 7. IC degradation using various control experiments as IC only, sunlight only, catalyst only and compared to the presence of both Sunlight and catalyst.

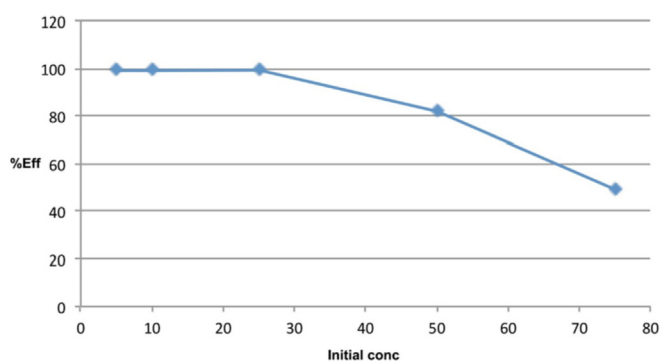

Fig. 8. Effect of initial IC dye concentration on the photocatalytic degradation efficiency of Ag@CaO in degradation of IC dye.

dark in the presence of catalyst. Noticeable reduction after 1hr in dye color was observed with only ≈75% decolorization efficiency. This indicates the adsorption of dye due to the high active sites of Ag@CaO surface. The degradation efficiency is 99.45% in the presence of Ag@CaO under sun light. Hence, from the photo catalytic experiments we can conclude that Ag@CaO in the presence of sun light is extremely effective as photocatalyst for IC degradation. In order to find the optimum conditions of the photocatalytic degradation, studying the different parameters such as initial dye concentration, catalyst doses, pH and temperature were optimized because these factors are effective in any water treatment process (Maroušek et al., 2019b).

3.2.1. Impact of initial concentration

The photocatalytic degradation was estimated by applying different concentrations of indigo carmine solutions 5, 10, 25, 50 and 75 ppm. High degradation effectiveness appeared at 5, 10 and 25 ppm IC concentrations after 25 min, as shown in Fig. 8. The degradation effectiveness is reduced as the original concentration increases to 50 and 75 ppm. This is owing to the dye molecules well adsorbed on the surface of catalyst at small levels followed by instant degradation. By comparison, when the catalyst dose and light intensity are continuous, overcrowding of dye molecules on the catalyst surface leads to a diminish in the rate of degradation. Furthermore, with high concentrations of dye, color intensity rises and light penetration decreases the amount of photons entering the surface of the substratum (Neppolian et al., 2002).

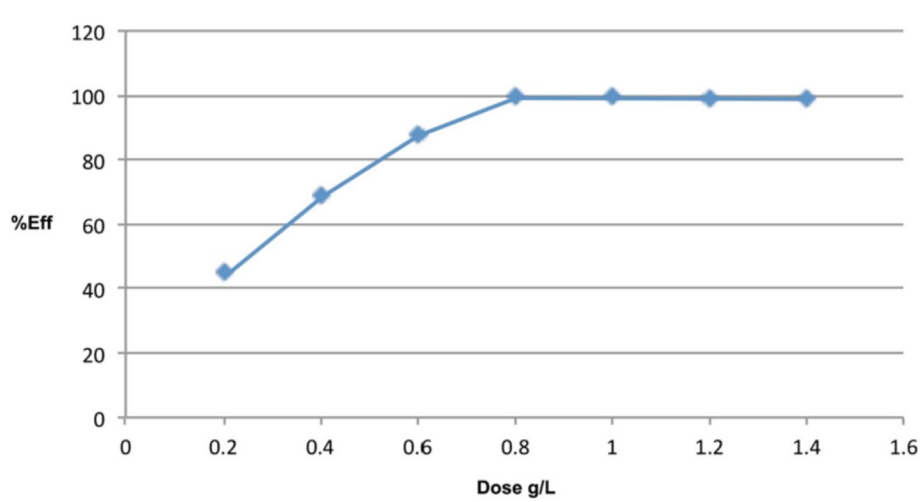

Fig. 9. Effect of the catalyst amount on the photocatalytic degradation efficiency of Ag@CaO in degradation of IC dye.

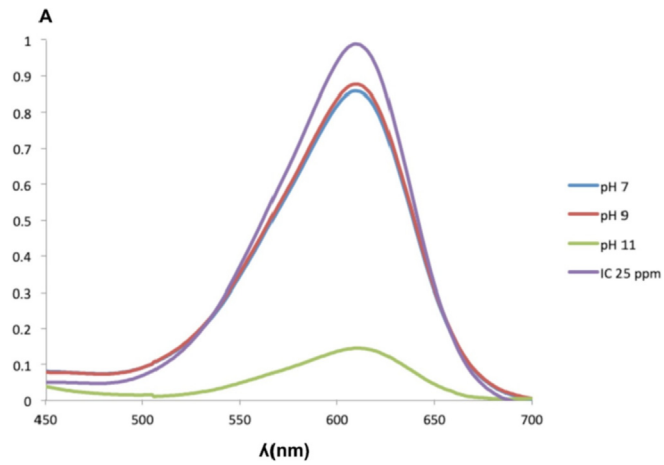

Fig. 10. pH-dependent variation in the absorption spectrum of IC during sunlight irradiation in the presence Ag@CaO composite.

Table 1
Antibacterial activity of CaO and Ag@ CaO nanoparticles substances against Gram-negative and Gram-positive bacteria.

Tested Bacteria	Inhibition zone diameter (mm) Average ±SD[a]	
	CaO	Ag@ CaO
Bacillus cereus	26.33 ± 1.52	29 ± 1
Bacillus subtilis	32.33 ± 3.78	36 ± 1
Enterococcus feacalis	34.33 ± 1.52	34 ± 1.73
E. coli	33 ± 1	39 ± 2.64
Klebsiella sp.	33.66 ± 0.57	36 ± 1
Pseudomonas fluorescence	26.33 ± 1.52	28.33 ± 2.08
Enterobacter sp.	24.33 ± 1.52	35 ± 2
Micrococcus leteus	27 ± 4.35	31 ± 4.35

[a] SD = standarddeviation

3.2.2. Influence of catalyst dose

In order to achieve the optimum catalyst quantity, different catalyst quantities, 0.20–1.4 g/L doses were used in distinct experiments maintaining both IC concentration (25 ppm) and contact time (25 min) are constants. Fig. 9 shows the relationship between the dosage of the catalyst and the effectiveness of photocatalytic degradation. As shown, the direct relationship between the dose of the catalyst and photodegradation effectiveness stays stable up to 0.8 g/L. Increased catalyst dosage of 0.2–0.8 g/L enhanced photocatalytic degradation owing to enhancement in active sites fitted for adsorption of dye molecules then OH^-producing (Subramani et al., 2007). The curve was near to saturation when the catalyst dose rose to 0.8 g/L. This result showed that this concentration could be supplied with the active sites adequate for adsorption of dye molecules.

3.2.3. Effect of pH

The impact of the pH on the IC photodegrdation was investigated at values 12 (natural pH), 9 and 7. HCl was used to control pH. Fig. 10 shows the absorption spectra of IC solutions with different pH values after irradiation time for 15 min with catalyst dose 0.8 g/L. At natural pH the efficiency of decolorization is found to be 85% while at pH 7 and 9, the resulted efficiencies were 15% and 14%, respectively. Photodegradation is not successful at low pH values due to dissolution of calcium oxide photocatalyst when HCl was added (Sarker, 2001) to adjust the pH values at pH at 9 and 7.

3.2.4. Effect of temperature

The impact of temperature on IC dye photocatalytic degradation was investigated at various temperatures, room temperature (25 °C), 35, 45, 55 and 65 °C. As a function of temperature, no notable variation in the effectiveness of IC decolorization is observed to be compared. It has been reported that photocatalytic degradation effectiveness is not temperature dependent (Sood et al., 2015).

3.2.5. Large-scale process

The reaction efficiency for large-scale reactions is sustained at approximately the same rate under whatever condition the large-scale is 50 times as high as the experimental scale. Therefore, the fabricated composite is a promising candidate for the potential applications in industrial.

3.3. Antibacterial activity

The antibacterial results of CaO and Ag@CaO against Gram-negative and Gram-positive bacteria are listed in Table .1 and illustrated in Fig. 11.

The subfigures 1,2,5 and 6 revealed moderate antibacterial

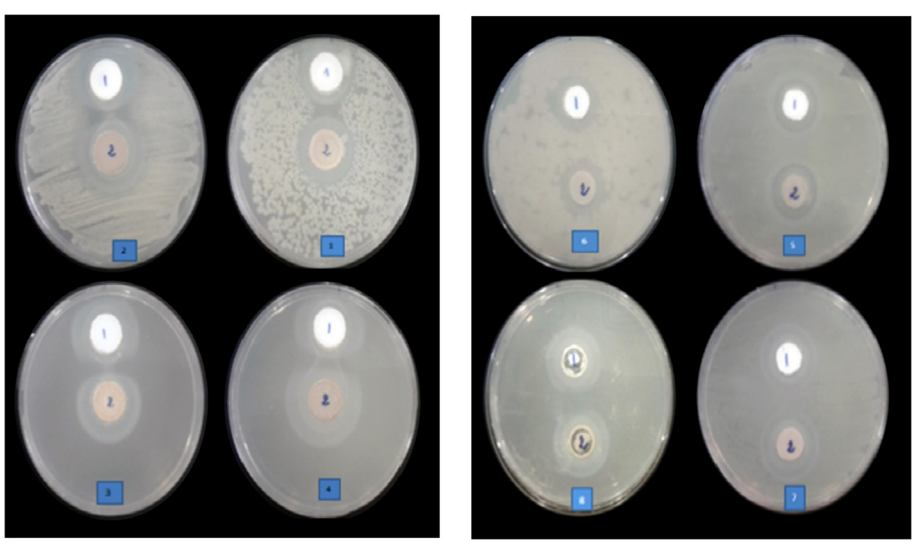

Fig. 11. Images of the antibacterial test results for Gram-negative and Gram-positive bacteria of pure CaO(1) and Ag@CaO composite (2).

activity against *Bacillus cereus, Bacillus subtilis*, *Klebsiella* sp., *and Pseudomonas fluorescence.* In contrast, the subfigures 3,4,7 and 8 display a strong bacteriocidal effect against *Enterococcus feacalis, E. coli, Enterobacter* sp ., *and Micrococcus leteus.*

CaO antibacterial activity may be due to the generation of superoxide ($\bullet O^{-2}$) and other reactive oxygen species (ROS) such as $HO^{\bullet 2}$, and H_2O_2 from the surface of calcium oxide. The radicals harm the cell membrane through reaction and break the structure of polyunsaturated phospholipids as many scientists have reported (Sawai, 2003; Sawai et al., 2001). On the other hand Ag@CaO, had higher antibacterial potential against Gram (+ve) and Gram (-ve) bacteria and acts as a powerful weapon against multidrug-resistant (MDR) bacteria such as *Pseudomonas aeruginosa,* ampicillin-resistant *Escherichia coli,* erythromycin-resistant *Streptococcus pyogenes,* methicillin-resistant *Staphylococcus aureus (MRSA)* and vancomycin-resistant *Staphylococcus aureus.* The higher activity of Ag@CaO may be due to high surface-to-volume ratios. As reported before (Percival et al., 2007; Rai et al., 2012), the presence of silver nanoparticles shows good interaction with bacteria and enhances the release of reactive oxygen species (ROS) on the surface.

4. Conclusions

In this work, we succeeded in achieving the desired goals by the conversion of chicken egg shell wastes collected at no cost to utilizable valuable material in wastewater treatment. We can verify, after thorough literature study, that this is the first time to use the calcium oxide generated from the egg shell as a photocatalyst. The loading of Ag nanoparticles on the surface of calcium oxide resulted in the formation of novel composite Ag-NPs@CaO. The materials showed strong photocatalytic performance for fast decoloration of indigo carmine dye in the presence of sunlight irradiation. It also showed powerful weapons against many types of bacteria, especially multidrug-resistant bacteria (MDR). These findings provide a facile, fast and inexpensive strategy for all those who are interested in industries which involve dyeing process. Additional studies on waste recycling relevant to bioactive products to be used in wastewater treatment are underway.

Declaration of competing interest

The authors certify that they have NO affiliations with or involvement in any organization or entity with any financial interest (such as honoraria; educational grants; participation in speakers' bureaus; membership, employment, consultancies, stock ownership, or other equity interest; and expert testimony or patent-licensing arrangements), or non-financial interest (such as personal or professional relationships, affiliations, knowledge or beliefs) in the subject matter or materials discussed in this manuscript.

Acknowledgment

The authors are grateful for the chemicals and laboratory facilities at Jouf University and for the support of the central laboratory, Jouf University for analysis.

References

Balázsi, C., Wéber, F., Kövér, Z., Horváth, E., Németh, C., 2007. Preparation of calcium phosphate bioceramics from natural resources. J. Eur. Ceram. Soc. 27, 1601–1606. https://doi.org/10.1016/j.jeurceramsoc.2006.04.016.

Barka, N., Assabbane, A., Nounah, A., Ichou, Y.A., 2008. Photocatalytic degradation of indigo carmine in aqueous solution by TiO_2-coated non-woven fibres. J. Hazard Mater. 152, 1054–1059. https://doi.org/10.1016/j.jhazmat.2007.07.080.

Boey, P.-L., Maniam, G.P., Hamid, S.A., 2011. Performance of calcium oxide as a heterogeneous catalyst in biodiesel production: a review. Chem. Eng. J. 168, 15–22. https://doi.org/10.1016/j.cej.2011.01.009.

Colombo, K., Ender, L., Barros, A.A.C., 2017. The study of biodiesel production using CaO as a heterogeneous catalytic reaction. Egypt. J. Pet. 26, 341–349. https://doi.org/10.1016/j.ejpe.2016.05.006.

Devarahosahalli Veeranna, K., Theeta Lakshamaiah, M., Thimmasandra Narayan, R., 2014. Photocatalytic degradation of indigo carmine dye using calcium oxide. Int. J. Photochem. 1–6. https://doi.org/10.1155/2014/530570, 2014.

Elaheh, M., 2013. Ultrasonic-assisted preparation of nano eggshell powder: a novel catalyst in green and high efficient synthesis of 2-aminochromenes. Ultrason. Sonochem. 20, 1436–1441. https://doi.org/10.1016/j.ultsonch.2013.04.00.

Essawy, A.A., Nassar, A.M., Arafa, W.A.A., 2018. A novel photocatalytic system consists of Co (II) complex@ ZnO exhibits potent antimicrobial activity and efficient solar-induced wastewater remediation. Sol. Energy 170, 388–397. https://doi.org/10.1016/j.solener.2018.05.073.

Evangelia, P., Nasia, K., Loukas, K., Panayiotis, K., Petros, N., Georgios, C., Ioannis, V., 2018. Turning calcined waste egg shells and wastewater to Brushite: phosphorus adsorption from aqua media and anaerobic sludge leach water. J. Clean. Prod. 178, 419–428. https://doi.org/10.1016/j.jclepro.2018.01.014.

Ferraz, E., Gamelas, J.A.F., Coroado, J., Monteiro, C., Rocha, F., 2018. Eggshell waste to produce building lime: calcium oxide reactivity, industrial, environmental and economic implications. Mater. Struct. 51, 115. https://doi.org/10.1617/s11527-018-1243-7.

Gabriele, D., Laura, M., Aida, M.C., Silvano, M., 2017. Recycling of eggshell waste into low-cost adsorbent for Ni removal from wastewater. J. Clean. Prod. 164, 1497–1506. https://doi.org/10.1016/j.jclepro.2017.07.085.

Geovania, C., Euzébio, S., Valderi, D.L., Marcelo, O.R., André, G., Mary, C.F.A., Julian, E., Rodrigo, J., 2018. Conversion of "waste plastic" into photocatalytic nanofoams for environmental remediation. ACS Appl. Mater. Interfaces 10, 8077–8085. https://doi.org/10.1021/acsami.7b19834.

Hassan, A.M., Nassar, A.M., Ibrahim, N.M., Elsaman, A.M., Rashad, M.M., 2013. An easy synthesis of nanostructured magnetite-loaded functionalized carbon spheres and cobalt ferrite. J. Coord. Chem. 66, 4387–4398. https://doi.org/10.1080/00958972.2013.867037.

Khemthong, P., Luadthong, C., Nualpaeng, W., Changsuwan, P., Tongprem, P., Viriya-Empikul, N., Faungnawakij, K., 2012. Industrial eggshell wastes as the heterogeneous catalysts for microwave-assisted biodiesel production. Catal. Today 190, 112–116. https://doi.org/10.1016/j.cattod.2011.12.024.

Kim, R., Park, J.-W., 2001. Effect of annealing on aging characteristics of MgO-CaO film as a protective layer for AC PDP. J. Mater. Sci. 36, 1475–1479. https://doi.org/10.1023/A:1017596729635.

Lorena, A., Irene, G., Laura, G., María, E., Ana, U., Paloma, F., Félix, A., 2019. New photocatalytic materials obtained from the recycling of alkaline and Zn/C spent batteries. J. Mater. Res. Technol. 8, 2809–2818. https://doi.org/10.1016/j.jmrt.2019.04.020.

Maroušek, J., Strunecký, O., Stehel, V., 2019. Biochar farming: defining economically perspective applications. Clean Technol. Environ. Policy 21, 1389–1395. https://doi.org/10.1007/s10098-019-01728-7.

Maroušek, J., Stehel, V., Vochozka, M., Kolář, L., Maroušková, A., Strunecký, O., Peterka, J., Kopecký, M., Shreedhar, S., 2019. Ferrous sludge from water clarification: changes in waste management practices advisable. J. Clean. Prod. 218, 459–464. https://doi.org/10.1016/j.jclepro.2019.02.037.

Nassar, A.M., 2018. Catalytic reactivity of new Ni (II), Cu (II) and Sn (II) complexes for decolorization of indigo carmine in aqueous solution, high efficiency of copper complex. Appl. Organomet. Chem. 32, e4056 https://doi.org/10.1002/aoc.4056.

Nassar, A.M., Elseman, A.M., Alsohaimi, I.H., Alotaibi, N.F., Khan, A., 2019. Diaqua oxalato strontium (II) complex as a precursor for facile fabrication of Ag-NPs@ $SrCO_3$, characterization, optical properties, morphological studies and adsorption efficiency. J. Coord. Chem. 72, 771–785. https://doi.org/10.1080/00958972.2019.1588964.

Nassar, A.M., Hassan, A.M., Alabd, S.S., 2015. Antitumor and antimicrobial activities of novel palladacycles with abnormal aliphatic CH activation of Schiff Base 2-[(3-phenylallylidene) amino] phenol. Synth. React. Inorganic, Met. Nano-Metal Chem. 45, 256–270. https://doi.org/10.1080/15533174.2013.831878.

Nassar, A.M., Zeid, E.F.A., Elseman, A.M., Alotaibi, N.F., 2018. A novel heterometallic compound for design and study of electrical properties of silver nanoparticles-decorated lead compounds. New J. Chem. 42, 1387–1395. https://doi.org/10.1039/C7NJ03682E.

Navaladian, S., Viswanathan, B., Viswanath, R.P., Varadarajan, T.K., 2007. Thermal decomposition as route for silver nanoparticles. Nanoscale Res. Lett. 2, 44. https://doi.org/10.1007/s11671-006-9028-2.

Neppolian, B., Choi, H.C., Sakthivel, S., Arabindoo, B., Murugesan, V., 2002. Solar/UV-induced photocatalytic degradation of three commercial textile dyes. J. Hazard Mater. 89, 303–317. https://doi.org/10.1016/S0304-3894(01)00329-6.

Oliveira, D.A., Benelli, P., Amante, E.R., 2013. A literature review on adding value to solid residues: egg shells. J. Cleaner prod. 46, 42–47. https://doi.org/10.1016/j.jclepro.2012.09.045.

Oppong, S.O.-B., Opoku, F., Govender, P.P., 2019. Tuning the electronic and structural properties of Gd-TiO_2-GO nanocomposites for enhancing photodegradation of IC dye: the role of Gd^{3+} ion. Appl. Catal. B Environ. 243, 106–120. https://doi.org/10.1016/j.apcatb.2018.10.031.

Peralta, M. de L.R., Sánchez-Cantú, M., Puente-López, E., Rubio-Rosas, E., Tzompantzi, F., 2018. Evaluation of calcium oxide in Rhodamine 6G photodegradation. Catal. Today 305, 75–81. https://doi.org/10.1016/j.cattod.2017.09.057.

Percival, S.L., Bowler, P.G., Dolman, J., 2007. Antimicrobial activity of silver-containing dressings on wound microorganisms using an in vitro biofilm model. Int. Wound J. 4, 186–191. https://doi.org/10.1111/j.1742-481X.2007.00296.x.

Rai, M.K., Deshmukh, S.D., Ingle, A.P., Gade, A.K., 2012. Silver nanoparticles: the powerful nanoweapon against multidrug-resistant bacteria. J. Appl. Microbiol. 112, 841–852. https://doi.org/10.1111/j.1365-2672.2012.05253.x.

Rashad, M.M., Hassan, A.M., Nassar, A.M., Ibrahim, N.M., Mourtada, A., 2014. A new nano-structured Ni (II) Schiff base complex: synthesis, characterization, optical band gaps, and biological activity. Appl. Phys. A 117, 877–890. https://doi.org/10.1007/s00339-014-8448-6.

Sarker, S.C., 2001. A method for separation of lime high or low calcium oxide containing limestone. Indian J. Chem. Technol. 8, 255–259. http://hdl.handle.net/123456789/22914.

Sawai, J., 2003. Quantitative evaluation of antibacterial activities of metallic oxide powders (ZnO, MgO and CaO) by conductimetric assay. J. Microbiol. Methods 54, 177–182. https://doi.org/10.1016/S0167-7012(03)00037-X.

Sawai, J., Shiga, H., Kojima, H., 2001. Kinetic analysis of death of bacteria in CaO powder slurry. Int. Biodeterior. Biodegrad. 47, 23–26. https://doi.org/10.1016/S0964-8305(00)00115-3.

Shaveisi, Y., Sharifnia, S., 2018. Deriving Ag_3PO_4CaO composite as a stable and solar light photocatalyst for efficient ammonia degradation from wastewater. J. energy Chem. 27, 290–299. https://doi.org/10.1016/j.jechem.2017.06.012.

Song, L., Zhang, S., 2010. A simple mechanical mixing method for preparation of visible-light-sensitive NiO-CaO composite photocatalysts with high photocatalytic activity. J. Hazard Mater. 174, 563–566. https://doi.org/10.1016/j.jhazmat.2009.09.088.

Song, L., Zhang, S., Chen, B., Sun, D., 2009. Highly active NiO-CaO photocatalyst for degrading organic contaminants under visible-light irradiation. Catal. Commun. 10, 421–423. https://doi.org/10.1016/j.catcom.2008.08.032.

Sood, S., Kumar, S., Umar, A., Kaur, A., Mehta, S.K., Kansal, S.K., 2015. TiO_2 quantum dots for the photocatalytic degradation of indigo carmine dye. J. Alloy. Comp. 650, 193–198. https://doi.org/10.1016/j.jallcom.2015.07.164.

Subramani, A.K., Byrappa, K., Ananda, S., Rai, K.M.L., Ranganathaiah, C., Yoshimura, M., 2007. Photocatalytic degradation of indigo carmine dye using TiO_2 impregnated activated carbon. Bull. Mater. Sci. 30, 37–41. https://doi.org/10.1007/s12034-007-0007-8.

Szoke, Á.F., Szabó, G.S., Hórvölgyi, Z., Albert, E., Gaina, L., Muresan, L.M., 2019. Eco-friendly indigo carmine-loaded chitosan coatings for improved anti-corrosion protection of zinc substrates. Carbohydr. Polym. 215, 63–72. https://doi.org/10.1016/j.carbpol.2019.03.077.

Witoon, T., 2011. Characterization of calcium oxide derived from waste eggshell and its application as CO_2 sorbent. Ceram. Int. 37, 3291–3298. https://doi.org/10.1016/j.ceramint.2011.05.125.

Yaling, L., Zhou, J., Yunde, F., Yong, Y., Bin, T., 2017. Preparation of environment-friendly 3D eggshell membrane-supported anatase TiO_2 as a reusable photocatalyst for degradation of organic dyes. Chem. Phys. Lett. 689, 142–147. https://doi.org/10.1016/j.cplett.2017.10.019.